Phase stability and low-temperature specific heat up to 14 T of $_{x}$ as a function of oxygen stoichiometry

Genoud, Jean-Yves; Mirmelstein, Alexey; Triscone, Gilles; Junod, Alain; Muller, Jean

How to cite

GENOUD, Jean-Yves et al. Phase stability and low-temperature specific heat up to 14 T of $_{x}$ as a function of oxygen stoichiometry. In: Physical review. B, Condensed matter and materials physics, 1995, vol. 52, n° 17, p. 12833–12843. doi: 10.1103/PhysRevB.52.12833

This publication URL: https://archive-ouverte.unige.ch/unige:93834

Publication DOI: 10.1103/PhysRevB.52.12833

Phase stability and low-temperature specific heat up to 14 T of $BaCuO_x$ as a function of oxygen stoichiometry

J.-Y. Genoud,* A. Mirmelstein,† G. Triscone, A. Junod, and J. Muller
Département de Physique de la Matière Condensée, Université de Genève, 24 quai Ernest-Ansermet, CH-1211 Genève 4, Switzerland
(Received 8 May 1995)

The stability of the $BaCuO_x$ ($x \geq 2$) phase has been mapped over a wide range of temperature (300–1100 °C) and oxygen pressure (10^{-5}–10^3 bar). At ambient pressure and temperature, $BaCuO_x$ is found to be in a metastable state: long annealing at 450 °C tends to decompose the phase into $Ba_2Cu_3O_5$ and BaO_2. Having obtained the phase stability domain in the $[T,p(O)_2]$ plane we were able to prepare single-phase samples of $BaCuO_x$ with different oxygen contents suitable for precise intrinsic thermodynamical measurements. We show that the behavior of the low-temperature specific heat ($1.1 \leq T \leq 32$ K) and its dependence on the magnetic field ($0 \leq B \leq 14$ T) may be understood by taking into account a many-level magnetic system directly related to the Cu_6O_{12} and $Cu_{18}O_{24}$ structural blocks of $BaCuO_x$. Depending on the oxygen concentration, competition between antiferromagnetic (AF) ordering and the many-level system is observed. With increasing oxygen content, the Néel temperature decreases whereas amplitude of the many-level system increases. The zero-field AF transition belongs to the three-dimensional isotropic Heisenberg universality class.

I. INTRODUCTION

In the quaternary phase diagram Y-Ba-Cu-O, $BaCuO_x$ is one of the phases in equilibrium with the high-T_c superconductor (HTSC) $YBa_2Cu_3O_{7-d}$ (Y123). The former compound, as well as Y_2BaCuO_5 or $Y_2Cu_2O_5$, are frequently encountered as impurities in Y123 and are known to affect the measured specific heat, magnetic susceptibility, etc.[1–3] In the present paper, we focus on the low-temperature thermodynamic properties of $BaCuO_x$.

In contrast to its simple chemical formula, $BaCuO_2$ has a rather complex body-centered-cubic structure (space group $Im3m$) with 90 formula units per unit cell.[4,5] The unit cell can be described with six lone CuO_4 units, eight Cu_6O_{12} ring clusters, and two $Cu_{18}O_{24}$ sphere clusters (see, e.g., Fig. 1 of Ref. 6 or Ref. 7 for a diagram). According to magnetization and neutron-diffraction measurements,[6] the Cu_6O_{12} and $Cu_{18}O_{24}$ clusters have ferromagnetic ground states with large spin, $s=3$ and 9, respectively. Below 15 K the Cu_6O_{12} rings order antiferromagnetically while the $Cu_{18}O_{24}$ clusters remain paramagnetic down to 2 K, and are supposed to exhibit novel magnetic properties at lower temperature in an external magnetic field.

The low-temperature specific heat of $BaCuO_x$ has been measured by several groups in relation to the specific heat of the Y123 compound.[1,8–11,3,12,13] Depending on the sample preparation, the specific heat showed different behaviors, with features such as an upturn at low temperature and/or a wide peak between 5 and 14 K. These differences have been attributed to different oxidation states,[1] but can also be due to impurities in some of the samples studied.

We present here a systematic investigation of single-phase $BaCuO_x$ samples with different oxygen contents $2 \leq x \leq 2.17$. In order to obtain pure samples, the phase diagram was carefully mapped over a wide range of temperature and oxygen pressure. The samples under study differ only by their oxidation state. The magnetic properties were investigated by measuring the low-temperature specific heat from 1.1 to 32 K in magnetic fields up to 14 T, and magnetization up to 5.5 T. An effective model of a many-level magnetic system is proposed to account for the low-temperature specific heat. This model is also in agreement with independent magnetization measurements. The zero-field antiferromagnetic (AF) ordering is analyzed in terms of critical behavior.

II. SAMPLE PREPARATION

The samples under study have been prepared by the solid-state reaction technique normally used to form HTSC copper oxides.[12,14] High-purity (99.999%) $BaCO_3$ and CuO powders were mixed in the stoichiometric ratio Ba:Cu=1:1, fired in flowing oxygen at ambient pressure between 880 and 900 °C for several days, and reground. This procedure was repeated until x-ray diffraction patterns indicated complete decomposition of the carbonate. The prereacted powders were cold pressed into pellets of about 0.5 g and 6 mm in diameter, fired in air at 950 °C for 48 h, slowly cooled, and finally annealed at 300 °C in pure oxygen flow for 2 days in order to homogenize the oxygen content. At this stage (sample code BCO), the samples were single phase according to optical micrographs, scanning electron microscopy (SEM), and x-ray analysis. Figure 1 shows the typical diffraction pattern recorded on a Bragg-Brentano diffractometer. Phase purity was checked by a Rietveld refinement [program DBWS-9006PC (Ref. 15)]. As shown in the upper pattern of Fig. 1, no impurity phase was detected. The macroscopic density of the samples exceeds 95% of the theoretical value, $\rho \approx 5.7$ g/cm^3.

The pellets from this homogeneous batch were then annealed separately at different temperatures ($300 \leq T \leq 1100$ °C) and pure oxygen pressures ($10^{-5} \leq p \leq 1180$ bar),[16] to modify the oxygen stoichiometry and to explore the

0163-1829/95/52(17)/12833(11)/$06.00

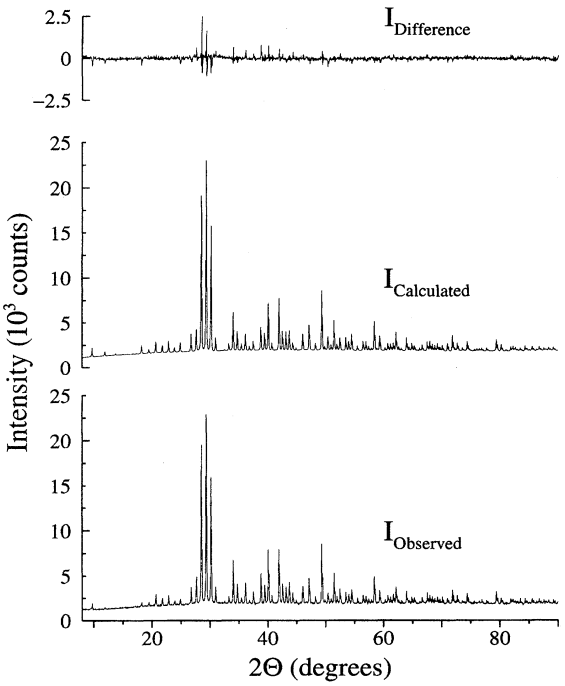

FIG. 1. Rietveld plots of sample BCO.

stability limits. Annealing times ranged from 1 to 48 days, depending on the expected kinetics of reaction. The high-temperature equilibrium state was frozen by quenching the samples into liquid gallium when annealing at 1 bar O_2 or below. Alternatively, a fast cooling rate was ensured by convection for high-pressure treatments.[16]

III. STABILITY AND CHARACTERIZATION

The possible existence of different phases in the Ba-Cu-O ternary system is still debated in the current literature (for a review, see Ref. 17). $BaCuO_2$, $BaCu_2O_3$, $Ba_2Cu_3O_5$, and Ba_2CuO_3 phases are commonly quoted, but additional stoichiometries have been proposed. At high temperature and 1 bar oxygen pressure, $BaCuO_2$ and CuO are the only phases along the BaO-CuO_x tie line.[14,18] According to a calculation based on thermodynamic data, the $BaCuO_2$ phase is stable only at intermediate temperature and oxygen pressure.[19] This stability range is crossed by the experimental solidus proposed by Lindemer, Washburn, and MacDougall.[20]

For the present study samples were synthesized in the stability region proposed by Voronin and Degterov,[19] close to the melting point. Eighteen combinations of temperature, oxygen pressure, and time were selected to vary the oxygen concentration and to explore the stability range. The annealing parameters, listed in Table I, are chosen both inside and outside the predicted stability range (Fig. 2). For example, samples annealed at low temperature ($T \leq 600$ °C) and high pressure [$p(O_2) \geq 1$ bar] are expected to decompose into $Ba_2Cu_3O_5$ and other phases. After these treatments, the samples were again characterized by x-ray analysis, optical micrographs, and SEM microscopy.

A. Characterization technique

The SEM is coupled with an energy-dispersive x-ray analysis (EDAX) system allowing the measurement of the

TABLE I. Annealing conditions, lattice constant, and oxygen concentration estimated from Eq. (2) of Ref. 20 for the $BaCuO_x$ samples investigated in this work. Asterisk on lattice parameters: high-accuracy data, see text.

Sample code no.	Annealing conditions $\log_{10}[p(O_2)$ (bar)]	T (°C)	Time (h)	Characterization a (Å)	Oxygen content x	Remarks
BCO	as sintered			18.3055(8)		Pure
918b	3.07	300	4	18.3081(9)	2.175	Partially decomposed
917d	2	300	96			Decomposed
917e	2	600	96			Decomposed
917a	1.57	300	72	18.3098(9)	2.168	Pure
917b	1.54	400	72	18.304(9)	2.158	Partially decomposed
916c	0	300	193	18.3071(2)*	2.16	Pure
918f	0	400	96	18.3093(8)	2.147	Pure
918d	0	450	1150	18.292(4)	2.14	Partially decomposed
916d	0	500	140	18.3079(9)	2.132	Pure
915d	0	700	28	18.2973(1)*	2.097	Pure
915a	0	900	25	18.2918(1)*	2.057	Pure
917f	0	1040	1			Melted
915b	−0.7	900	25	18.302(1)	2.04	Pure
97a	−2	950	25			Melted
916d	−3	500	162	18.290(1)	2.09	Pure
98a	−3	950	25			Melted
916a	−5	500	160	18.28573(8)*	2.05	Pure
918c	−5	700	110	18.2796(5)*	≈2	Pure

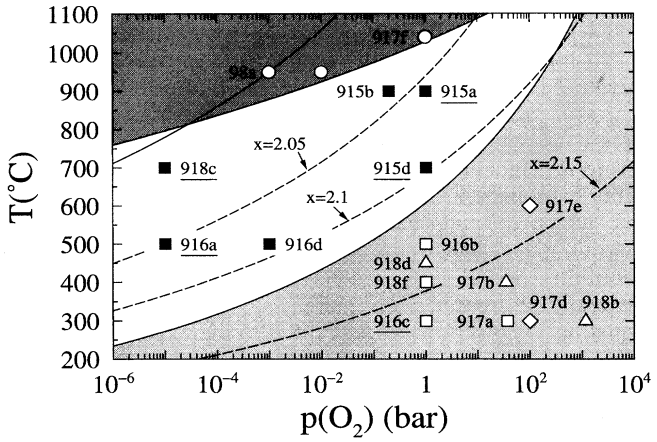

FIG. 2. Location of the various $BaCuO_x$ samples in the $p(O_2)$-T equilibrium diagram. The predicted stability domain of $BaCuO_x$ (Ref. 19) is bordered by the lower gray region and by the full line through sample 98a. The upper gray region is bordered by the solidus line (Ref. 20). The locus of equal oxygen concentration is shown by dashed lines for $x=2.05$, 2.1, and 2.15 (Ref. 20). Each symbol indicates the oxygen pressure and the annealing temperature prior to quenching. Squares: single phase $BaCuO_x$. Triangles: partially decomposed samples. Diamonds: completely decomposed samples showing no residual $BaCuO_x$. Circles: melted samples. Full symbols: samples within the predicted stability limits. Outside of this region (open symbols), the crystal structure is expected to depend on the annealing time.

cation stoichiometry. CuO and a single crystal of BaF_2 were used as external standards. The stoichiometry was determined by averaging at least five acquisitions on similar grains.

X-ray diffraction patterns were recorded with a Guinier camera and Cu $K\alpha_1$ radiation. The lattice parameters were determined by least-squares fitting, taking into account 50 reflections in the range $20° \leq 2\theta \leq 70°$. Silicon was added as an internal standard ($a=5.4308$ Å). The lattice parameters of five samples labeled by full squares in Fig. 2 (and with an asterisk in Table I) were determined with a higher accuracy using a Bragg-Brentano diffractometer and high-angle diffraction patterns, $45° \leq 2\theta \leq 120°$. The positions of the peaks were refined using a Voigt profile, and corrected with a second-order polynomial. These five samples were selected for the investigation of thermal and magnetic properties.

B. Phase stability

Our investigation confirms the experimental solidus line proposed by Lindemer, Washburn, and MacDougall[20] since samples 917f, 97a, and 98a melted (Fig. 2 and Table I). The samples annealed at $T \leq 900$ °C and $p \leq 1$ bar O_2 for one week turned out to be single-phase $BaCuO_x$; they are marked as pure in Table I and Fig. 2. Figure 3(a) shows a typical optical micrograph for a single-phase sample after annealing.

Sample 916c, annealed at 300 °C and 1 bar O_2 for 8 days, does not show any decomposition although it lies outside the expected stability range.[19] The following test shows that it is indeed metastable. After a long annealing (48 days) at a somewhat higher temperature (450 °C, 1 bar O_2), we could observe the incipient transformation proposed by Voronin and Degterov.[19] X-ray diffraction obtained after this long heat treatment (sample 918d) shows persisting $BaCuO_x$ phase together with broad peaks characteristic of $Ba_2Cu_3O_x$. The decomposition appears clearly in the micrographs. As compared to a single-phase $BaCuO_x$ sample [Fig. 3(a)] all grains in Fig. 3(b) are surrounded by dark rings which are confirmed to be $Ba_2Cu_3O_x$ by EDAX (Fig. 4). In partially decomposed samples, the $BaCuO_x$ phase exists both in a stoichiometric and an apparently Ba-deficient form.

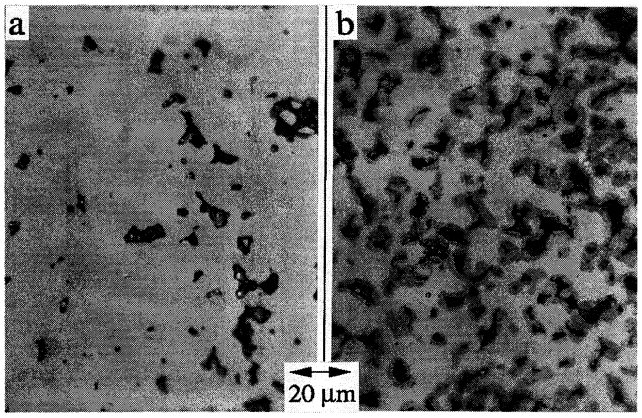

FIG. 3. (a) Optical micrograph of the pure sample 915a; the dark regions are pores. (b) Partially decomposed sample 918d; the pores are surrounded by a dark phase identified as $Ba_2Cu_3O_x$.

Annealing at 100 bar O_2 and 300 °C leads to the decomposition of $BaCuO_x$ into Ba-deficient and Ba-rich compounds (sample 917d), according to EDAX analysis. Further annealing of this partially decomposed sample at 600 °C tends to form $Ba_2Cu_3O_5$ and BaO_2 (sample 917e). X-ray diffraction patterns confirm the presence of badly crystallized $Ba_2Cu_3O_5$.

The results of the present study, which overlay an essential area of the $BaCuO_x$ stability range as well as the high-temperature phase diagram obtained experimentally in Refs. 14 and 18, agree with the phase diagram of the Ba-Cu-O system predicted by Voronin and Degterov.[19] We have shown that the $Ba_2Cu_3O_x$ phase appears at low temperature and high pressure (≥ 1 bar O_2). A very long annealing time is required to decompose our $BaCuO_x$ samples, presumably owing to their high density. At low temperature, metastable single-phase $BaCuO_x$ may persist even after annealing one week at 300 °C and 1 bar O_2 (sample 916c).

C. Cation stoichiometry of the $BaCuO_x$ phase

The cation stoichiometry obtained by a Rietveld refinement is Ba:Cu=1:1.05(2) in the initial batch BCO (Fig. 1), in reasonable agreement with the starting composition Ba:Cu =1:1. After annealing, EDAX measurements on the single-phase samples give the cation stoichiometry Ba:Cu =1:0.96(5) (Fig. 4). Chemical analysis leads to Ba:Cu =1:1.006(10). These results show that there is no significant variation of the cation stoichiometry due to the annealing as compared to the initial BCO batch. We conclude that all pure

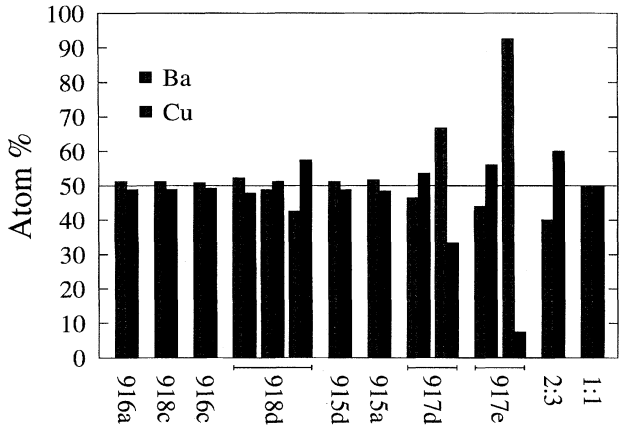

FIG. 4. Histogram of the EDAX local composition measurements. Annealing temperature and pressure increase from left to right; in multiphase samples (918d, 917d, and 917e) compositions in different locations are shown. The last two pairs of columns represent the ideal stoichiometric ratios for the $Ba_2Cu_3O_5$ and $BaCuO_2$ phases, respectively.

samples have the cation stoichiometry Ba:Cu=1:1. The nonstoichiometric $Ba_{0.92}Cu_{1.06}O_{2.14}$ composition found by Paulus and co-workers[7] for a single crystal is not confirmed. Ba deficiency often results from Al contamination during the melting process in Al_2O_3 crucibles. No Al was detected in our samples, either by EDAX or by chemical analyses. The apparent Ba deficiency in partially decomposed samples 918d and 917d (Fig. 4) is due to averaging in samples with incipient $BaCuO_x \rightarrow Ba_2Cu_3O_5 + \cdots$ transformation, as confirmed by further annealing (sample 917e; see Fig. 4).

D. Oxygen content of the $BaCuO_x$ phase

Based on the previous study, we could choose single-phase samples with oxygen concentrations covering almost the whole stability range for further investigation of physical properties. These samples are 918c, 916a, 915a, 915d, and 916c. The unit-cell volume is known to increase with oxygen content.[9] The values of the oxygen content given in Table I are not measured, but calculated using the semiempirical chemical thermodynamic representation given in Ref. 20. Based on this equation, the oxygen content of our $BaCuO_x$ samples change from $x=2$ (or less) to 2.168. The latter oxygen content seems to be very close to the upper limit for the $BaCuO_x$ phase. For example, sample 918b annealed at high pressure has probably a higher oxygen content but is already partially decomposed. Weller and Lines[21] attribute this excess oxygen to the O(6) sites in the lone CuO_4 units. This question is, however, not settled; see, for example, Ref. 7.

IV. EXPERIMENTAL RESULTS

A. Magnetic susceptibility

The magnetic susceptibility of five $BaCuO_x$ samples (namely, samples 916c, 915d, 915a, 916a, and 918c) was measured using a superconducting quantum interference device (SQUID) magnetometer from 5 to 300 K with an external magnetic field of 20 kOe (Fig. 5). Note that in this section we use the cgs system where $B[\mathrm{G}]=\mathrm{H[Oe]}+4\pi M[\mathrm{G}]$ and $\chi_v = M[\mathrm{emu/cm^3}]/H = \rho[\mathrm{g/cm^3}]\chi_g[\mathrm{emu/g}]$.

At high temperature, the temperature dependence of the susceptibility tends to follow the Curie-Weiss law $1/\chi=(T-\theta)/C$ for all five samples. The positive Curie-Weiss temperature shows that the predominant interactions are ferromagnetic (FM). At $T \leq 150$ K, the inverse susceptibility exhibits a positive curvature vs temperature. AF ordering, which certainly exists in the samples under study (see below), gives a negligible contribution to the magnetic susceptibility for all oxygen concentrations. The susceptibility generally decreases with increasing oxygen content. The equation $1/\chi=(T-\theta)/C$ was fitted to the experimental data from 190 to 300 K; $C=N_A n_s M \mu_B^2 p_{\mathrm{eff}}^2/3k_B$ where N_A is Avogadro's number, $n_s=1$ is the number of spins (i.e., of Cu ions) per formula unit, $M=233$ g/mol is the molar mass, and p_{eff} is the effective magnetic moment per Cu atom in units of μ_B. The fitted parameters are given in Table II; examples of fits are shown in Fig. 5 for samples 918c and 915d. All samples have a positive Curie-Weiss temperature near 50 K and Curie constants ranging from 0.38 to 0.47 emu K/mol Cu. The effective moment decreases from $1.86\mu_B$ to $1.68\mu_B$ with increasing oxygen content (Table II), or equivalently with increasing cell volume (inset of Fig. 5). The values of p_{eff} represent 88% to 98% of the value $1.9\mu_B$ expected for free Cu^{2+} ions. This shows that almost all copper atoms in the structure contribute to the magnetic susceptibility at high temperature.

As a whole, the magnetic susceptibility in the range $5<T<300$ K is not much affected by variations of the oxygen content. A similar behavior of $\chi(T)$ was reported by Wang *et al.*[6] for a sample fired at 925 °C and slowly cooled under He gas, i.e., for a low oxygen content. Based on magnetization and neutron-diffraction data, Wang *et al.*[6] argue that the Cu_6O_{12} and $Cu_{18}O_{24}$ clusters have ferromagnetic ground states with spin $s=3$ and 9, respectively. This assumption will be used in our further analysis.

B. Low-temperature specific heat

The specific heat of $BaCuO_x$ samples was measured using thermal relaxation calorimetry between 1 and 32 K.[12] The

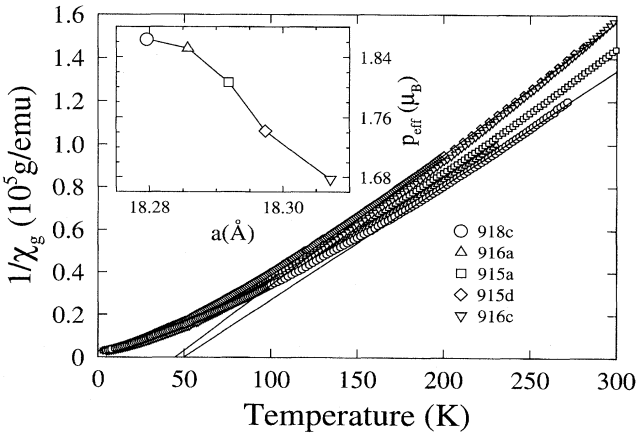

FIG. 5. Inverse magnetic susceptibility measured in a magnetic field of $H=20$ kOe ($B=2$ T). The two full lines are high-temperature Curie-Weiss fits for samples 918c and 915d. Inset: effective magnetic moment on Cu atoms vs cell parameter.

TABLE II. Curie constant C, Curie-Weiss temperature θ, and effective magnetic moment p_{eff} per Cu atom. The mole is defined as $BaCuO_2$.

Sample	C (emu K/mol Cu)	θ (K)	p_{eff} (μ_B)
916c	0.384	62	1.68
915d	0.414	45	1.74
915a	0.445	48	1.81
916a	0.468	46	1.85
918c	0.474	50	1.86

accuracy, tested with pure Cu and Ag, is $\pm 2\%$ for $T=1.5$–30 K and magnetic fields $B=0$–14 T. The typical sample mass was 10 mg. Data are normalized to a mole formula unit of $BaCuO_2$ (232.9 g), or to a gram-atom of $\frac{1}{4}$ $BaCuO_2$ (58.2 g) neglecting variations of the oxygen stoichiometry. The five samples 916c, 915d, 915a, 916a, and 918c were measured in zero magnetic field. We measured additionally the zero-field specific heat of the as-sintered BCO sample (see Table I). The specific heat of samples 918c and 916c, with the lowest and highest oxygen content, respectively, was measured in fields $B=0$, 5, 10, and 14 T. The contribution to the specific heat resulting from the hyperfine splitting of ^{63}Cu and ^{65}Cu nuclei was subtracted from the experimental data.[22]

Figure 6 presents all zero-field measurements in a C/T vs T^2 plot. Above 15 K the phonon contribution dominates for all samples. It can be represented by the usual expansion $C_{\text{lat}}=\alpha T^3+\beta T^5+\delta T^7$, where $\alpha=(\frac{12}{5})N_A k_B \pi^4 \Theta_D^{-3}$ (for 1 g-at.) and Θ_D, the Debye temperature, is about 144 K. Parameters β and δ depend on the shape of the phonon spectrum at medium wavelengths. Alternatively, the data above 15 K would suggest a representation including a simple cubic phonon term αT^3 and a huge linear term $\gamma \approx 60$ mJ/(K^2 mol); but this interpretation is not physically founded for an insulator. In any case, the specific heat of $BaCuO_x$ is much larger than that of $YBa_2Cu_3O_{7-d}$,[3,12] (see the lower curve of Fig. 6),[23] and, as an impurity, would affect the heat capacity of $YBa_2Cu_3O_{7-d}$ for any value of x.

The specific heat of samples 918c, 916a, 915a, and 915d reveals a sharp peak at a temperature that depends on the oxygen content: the higher the oxygen content, the lower the transition temperature. This transition corresponds to the antiferromagnetic ordering observed by Wang *et al.*[6] The inset of Fig. 6 shows the variation of the Néel temperature T_N taken as the temperature of the maximum of C/T, versus the lattice constant, i.e., the oxygen content. In comparison, previous measurements by Ramirez *et al.*[24] and Kuentzler *et al.*[10] showed broad anomalies between 9 and 13 K. Sample 916c with the highest oxygen content does not show any peak, but rather a strong upturn at low temperatures. Note that the specific heat of the as-sintered BCO sample does not show such a well-defined behavior; this can be attributed to oxygen inhomogeneity in the only sample cooled without quenching. This sample will be excluded from further discussion; it appears that careful control of the oxygenation process of the $BaCuO_x$ compound is of great importance, and that the quenching technique provides samples with better defined physical properties.

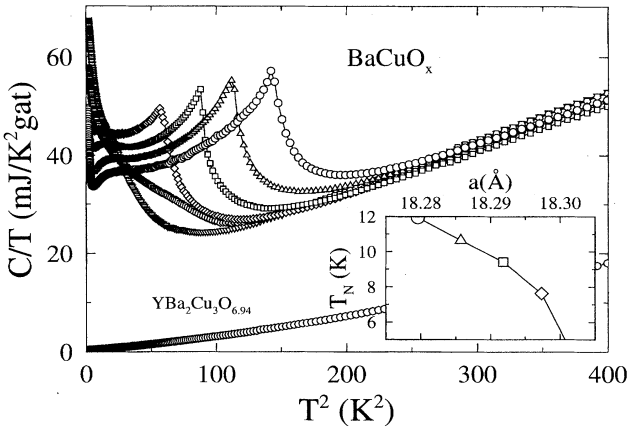

FIG. 6. Specific heat of $BaCuO_x$ samples with different oxygen concentrations. Symbols as for Fig. 5 with the addition of the as-sintered sample BCO appearing between the 916c and 915d curves. The specific heat of the superconductor $YBa_2Cu_3O_{6.94}$ is given for comparison (Ref. 23), lowest curve. Inset: Néel temperature versus lattice constant.

All curves in Fig. 6 behave similarly at low temperature with the presence of a broad Schottky-like specific heat. In the C/T vs T^2 representation, one would tend to distinguish a hump near 5 K and an upturn at $T \rightarrow 1$ K; but the upturn disappears in the C vs T representation (see Fig. 9 below) and both features can be described by a simple Schottky multilevel system. The amplitude of this contribution increases with oxygen content.

Figure 7 shows the effect of a magnetic field on the low-temperature Schottky-like anomaly (an enlargement of the low-temperature part is given in the inset). Similar results in $B=0$ and $B=6$ T were obtained by Sasaki *et al.*,[11] and in $B=0$ and $B=4$ T by Ahrens *et al.*[8] As expected, the magnetic field shifts the entropy change of the many-level system to higher temperatures, thus increasing the specific heat at high temperatures. A remarkable feature is that the first 5 T have a much more pronounced effect at high temperature than further increases of the field up to 14 T. The most visible manifestation of this effect appears as a quasilinear term that separates the zero-field C/T vs T^2 curve at $T>10$ K from those obtained in nonzero magnetic fields (Fig. 7). At $T=10$ K the difference $[C(B=5\text{ T})-C(B=0)]/T$ is 5.7 mJ/(K^2 g-at.). The differences between specific-heat values taken at 5, 10, and 14 T turn out to be smaller by an order of magnitude. The shift of the maximum of the Schottky-like anomaly and the variation of its amplitude with the field will be discussed in detail below.

Figure 8 shows the effect of a magnetic field on the specific heat of sample 918c with the highest AF transition temperature. As commonly observed, the Néel temperature decreases with increasing magnetic field; this is presented here for $BaCuO_x$. As for the low-temperature Schottky-like anomaly, the effect of the magnetic field does not qualitatively differ from that observed for sample 916c without AF transition. In particular, the specific heat at high temperature increases for low fields and progressively saturates. The quasilinear term induced by the field noted in sample 916c is also observed here, both above and below the Néel tempera-

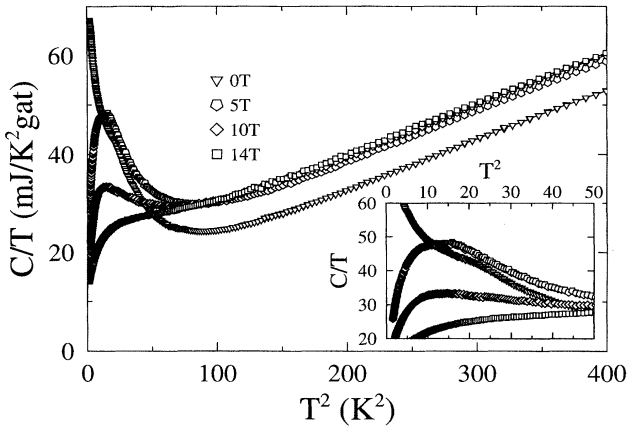

FIG. 7. Specific heat of oxidized sample 916c, which does not order antiferromagnetically, for different magnetic fields in a C/T vs T^2 representation. Inset: expanded low-temperature part.

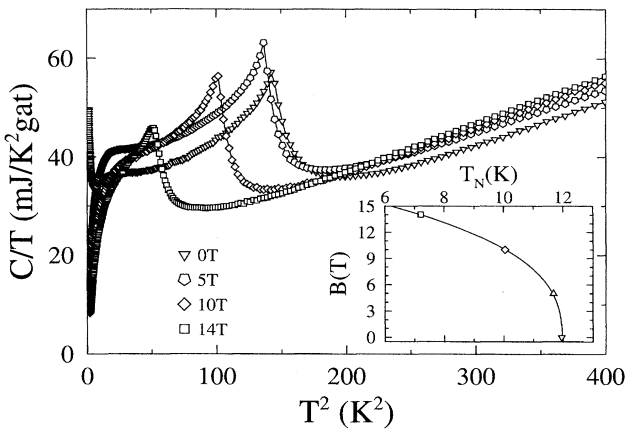

FIG. 8. Specific heat of low-oxygen sample 918c, which has the highest Néel temperature, for different magnetic fields. Inset: Néel temperature versus magnetic field and fit to a series expansion $T_c(B)/T_c(0)=1+aB^2+bB^3$ with $T_c(0)=11.97$ K, $a=-0.51$ mK/T^2, $b=-0.11$ mK/T^3, showing that the initial change is quadratic in B.

ture. Its presence explains why the peak of the C/T curve measured in zero field appears to be rather low compared to higher fields.

V. DISCUSSION

The specific-heat measurements described in the previous section show that the magnetic properties $BaCuO_x$ are rather complicated. First, an increase of the oxygen content decreases the Néel temperature and leads to complete suppression of the AF order in the fully oxygenated sample 916c. A magnetic field, as expected, decreases the AF transition temperature. The second feature is a low-temperature Schottky-like contribution that can be attributed to some many-level magnetic system. From the experimental data given in Figs. 6–8, it is seen that the amplitude of this Schottky-like anomaly depends upon the oxygen content whereas the position of the maximum, i.e., the energy splitting in zero field, does not. A final important remark is that the effect of the magnetic field on this anomaly in the samples with the highest and lowest oxygen concentration seems to be qualitatively the same. In contrast to the case of the AF transition, the magnetic field shifts the entropy involved in the many-level system towards higher temperatures. Hence there are two different magnetic subsystems in $BaCuO_x$, namely, the subsystem of spins that undergoes the AF transition on the one hand, and a subsystem of weakly interacting spins that gives rise to the Schottky-like anomaly on the other hand. Their different dependencies upon the oxygen concentration suggest that there is some competition between these two subsystems.

A. Magnetic entropy

In order to understand the origin of the many-level magnetic system in $BaCuO_x$, we best turn to entropy considerations. For a many-level system of spin s the total entropy S (per mole) is

$$S=nR\ \ln(2s+1)=\int_0^\infty \frac{C_{\mathrm{mag}}}{T}dT, \qquad (1)$$

where n is the number of many-level systems per formula unit and C_{mag} is the corresponding magnetic contribution to the specific heat. A rough estimation of the magnetic entropy involved in the low-temperature specific heat of sample 916c (which does not order), gives $S\approx 1600$ mJ/(K mol)$=400$ mJ/(K g-at.) (for this estimation, we have subtracted the lattice contribution extrapolated from above 15 K as described in Sec. IV B). Following Ref. 6, we assume that the spin of the $Cu_{18}O_{24}$ spheres in the $BaCuO_x$ structure is $s=9$ whereas that of the Cu_6O_{12} rings is $s=3$. Therefore the maximal expected entropy related to these magnetic clusters is of the order of $S=(2/90)R\ \ln(19)+(8/90)R\ \ln(7)\approx 2000$ mJ/(K mol)$=500$ mJ/(K g-at.), i.e., reasonably close to the experimental value. It shows that the low-temperature specific heat of $BaCuO_x$ can be, in principle, described in terms of a many-level magnetic system, i.e., a system with a large spin, directly related to structural blocks. We shall show that such an effective model can be parametrized and used to analyze the low-temperature specific heat of $BaCuO_x$ in more detail. We shall start with sample 916c, free of AF order, in zero field. We shall then refine the model to describe the dependence of the low-temperature specific heat upon both magnetic field and oxygen concentration, and find support from independent measurements of the magnetization as a function of field and temperature. Finally, we shall explore an effective description of the Schottky-like anomaly in order to analyze the type of AF order in those $BaCuO_x$ samples where the AF transition is well defined.

B. Schottky multilevel system: Sample without long-range AF order

To simplify further calculations we make two additional assumptions. First, we have to assume that in zero external field the degeneracy of the many-level system is partially removed by a weak spin-orbit coupling or/and molecular field, so that the zero-field specific heat can be described effectively as a *three-level system*. It does not imply, how-

ever, that the *actual many-level system* in zero field consists of *exactly three levels*. Second, we have to assume that the degeneracy factors of the levels lifted by internal interactions are relatively large, so that when an external magnetic field is applied any further energy splitting of these excited levels can be well approximated by a continuum, i.e., by a pseudospin band. Hence the corresponding contribution to the specific heat can be described by a linear term coming from this pseudoband, and it is expected to increase with magnetic field as does the number of excited levels inside a pseudoband.

Along these lines, the total specific heat can be written as

$$C = C_{\text{lat}} + C_{\text{Sch}} + C_{\text{lin}} \tag{2}$$

with the lattice contribution $C_{\text{lat}} = \alpha T^3 + \beta T^5 + \delta T^7$, the linear magnetic term $C_{\text{lin}} = \gamma T$, and the three-level Schottky specific heat C_{Sch}

$$C_{\text{Sch}} = N \frac{N_A}{k_B T^2} \frac{\Sigma_{i=1}^{2} g_0 g_i e_i^2 \exp(-e_i/k_B T) + g_1 g_2 (e_1 - e_2)^2 \exp[(e_1 + e_2)/k_B T]}{\left\{ \Sigma_{i=0}^{2} g_i \exp\left(-\frac{e_i}{k_B T} \right) \right\}^2} \tag{3}$$

with N_A Avogadro's number, N the number of three-level systems, g_i ($i=0,1,2$) the degeneracy factors of the levels with energies e_i ($e_0=0$ for the ground state), k_B Boltzmann's constant, and T the temperature.

Equation (2) was fitted to all specific-heat data described in Sec. IV B. In a first step, the zero-field data for the sample 916c were treated. The fitted parameters were α, β, δ, N, e_1, e_2, and γ; g_0, g_1, and g_2 were obtained by successive trials, enforcing the condition $g_0 + g_1 + g_2 = 2s + 1 = 19$. The fitted values of these parameters are given in Table III. It is necessary to emphasize that the fitted value of γ is essentially 0. In order to fit the specific heat of sample 916c at magnetic fields of 5, 10, and 14 T, the lattice contribution was frozen to its zero-field value, as well as the number of three-level system N, whereas g_i, e_i, and γ were allowed to vary independently.

Figure 9 shows the result of the fitting procedure. Table III lists all fitted parameters. As expected, a linear term appears and increases with field. The relative difference between fit and data is shown in the inset of Fig. 9, and does not exceed 3% over most of the temperature range. This supports the suggested effective model of a many-level magnetic system, for the sample without AF transition. It should be emphasized that the introduction of the linear term is required not only to bring data and model into agreement, but also to satisfy the condition of equal entropy at all fields. This latter condition strongly restricts the choice of suitable models. We do not claim, however, that the proposed model is a unique and exact microscopic description of the magnetic state of $BaCuO_x$. This is merely the simplest phenomenological model that accounts for the experimental results. For example, there is some freedom in fitting the value of spin s, or equivalently the total number of levels $2s+1$. We find that $s=9$ provides a rather good fit. This value coincides with the total spin of $Cu_{18}O_{24}$ structural blocks.[6] In principle the Schottky-like anomaly can also contain a contribution from the Cu_6O_{12} clusters. Other values of spin are not excluded as long as they are large. We emphasize that the degeneracy factors and energy levels resulting from the fit can hardly be considered as microscopic parameters.[25] They should rather be considered as *a first approximation* of the magnetic state of $BaCuO_2$ useful from the point of view of specific heat, and giving a better insight into the main physical features.

In order to further establish the experimental basis of this model, in particular the appearance of a magnetic-field-induced linear term, we measured the magnetization of samples 916c and 918c. The isothermal magnetization vs field was measured from 3 to 100 K and 0.5 to 5.5 T. Integrating the Maxwell relation

$$\left(\frac{\partial S}{\partial H} \right)_T = \left(\frac{\partial M}{\partial T} \right)_H \tag{4}$$

we compared the difference between specific-heat measurements at $B=0$ and a given field B [left-hand side of Eq. (5)] with the same value calculated from magnetization measurements [right-hand side of Eq. (5)]:

$$\frac{C(B=5\ \text{T}) - C(B=0)}{T} = \frac{\partial^2}{\partial T^2} \int_0^{5\ \text{T}} M\, dB. \tag{5}$$

Figure 10 shows that the magnetic data confirm the presence of a magnetic-field-induced linear term $\gamma(B)T$ with the correct order of magnitude at $T > 8-10$ K. According to the magnetic measurements, the pseudolinear term decreases near 30 K (the upper limit of the specific-heat measurements) and vanishes at 50 K. This vanishing is required by entropy considerations. The same procedure was applied to sample 918c (Fig. 10). Again, magnetic measurements agree with specific-heat data. The AF transition is clearly seen as a discontinuity at 12 K only in the latter data, however. The magnetic linear term is smaller in this case (compare also Figs. 7 and 8).

C. Schottky multilevel system: Samples with long-range AF order

We now apply the above model to the samples with lower oxygen concentrations. In fact, the same scheme of levels as discussed above is able to describe qualitatively the low-

TABLE III. Néel temperature T_N, coefficients of the lattice specific heat α, β, and δ entropy in the Schottky contribution $S_{\rm Sch}$, antiferromagnetic entropy up to the Néel point S_{T_N}, antiferromagnetic entropy up to 20 K $S_{\rm AF}$, fraction of the Cu_6O_{12} rings that participate in the Schottky anomaly $(S_{\rm Sch}-S_{\rm spheres})/S_{\rm rings}$, fraction of Cu_6O_{12} rings that do not order antiferromagnetically $1-S_{\rm AF}/S_{\rm rings}$, ratio of the critical amplitudes of the specific heat at the AF transition A^+/A^- [Eq. (6)], prefactor NN_Ak_B, energy levels e_i, and degeneracy factors g_i of the Schottky contribution [Eq. (3)] and coefficient of the quasilinear term γ [Eq. (2)]. See text for details.

Sample code	918c	916a	915a	015d	916c			
B (T)	0	0	0	0	0	5	10	14
T_N (K)	11.95	10.65	9.42	7.63				
α [mJ/(K^4 g-at.)]	0.164	0.163	0.159	0.161		0.165		
β [μJ/(K^6 g-at.)]	−0.109	−0.102	−0.101	−0.104		−0.0992		
δ (nJ/(K^8 g-at.)]	0.0371	0.0321	0.0312	0.0323		0.0291		
$S_{\rm Sch}$ [mJ/(K g-at.)]	200	217	238	245	344			
S_{T_N} [mJ/(K g-at.)]	165	144	123	80				
$S_{\rm AF}$ [mJ/(K g-at.)]	200	181	157	122				
$(S_{\rm Sch}-S_{\rm spheres})/S_{\rm rings}$ (%)	18	22	28	30	58			
$1-S_{\rm AF}/S_{\rm rings}$ (%)	44	50	56	66	≈90			
A^+/A^-	1.60±0.05	1.38±0.1	1.57±0.15	1.67±0.2				
NN_Ak_B [mJ/(K g-at.)]	90±10	98±10	107±10	110±10		155±2		
e_1/k_B (K)	5.53	5.53	5.53	5.53	5.53	7.92	8.35	10.04
e_2/k_B (K)	18.52	18.52	18.52	18.52	18.52	19.23	22.22	20.55
g_0	2	2	2	2	2	2	2	2
g_1	4	4	4	4	4	3	2	1
g_2	13	13	13	13	13	7	4	2
γ [mJ/(K^2 g-at.)]	0	0	0	0	0	5.74	6.41	7.59

temperature specific heat of the samples 915d, 915a, 916a, and 918c, with the same energy levels and degeneracy factors. The linear term is essentially zero in zero field. For each of these samples it is possible to fit simultaneously the Schottky-like contribution at low temperatures and the lattice contribution at $T>15$ K by adjusting only the NN_Ak_B prefactor of the Schottky term, Eq. (3), and the three lattice coefficients. The values obtained are given in Table III. The upper panel of Fig. 11 shows the decomposition of the measured specific heat for sample 915a according to Eq. (2). The lattice contribution remains almost unchanged for all samples, whereas the NN_Ak_B prefactor, i.e., the number of many-level systems, is found to decrease with decreasing oxygen concentration.

After having subtracted the lattice and Schottky contributions thus determined, we are left with the specific heat $C_{\rm AF}$ due to antiferromagnetic ordering for each oxygen concentration (lower panel of Fig. 11). Again, this separation is not exact, but leads to a reasonable approximation.

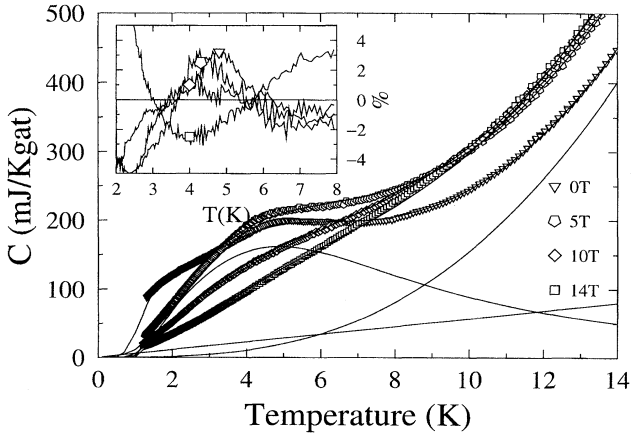

FIG. 9. Comparison of the specific-heat data for sample 916c, which does not order antiferromagnetically, in various fields (symbols) with the fitted model, Eq. (2) (lines through the symbols). For the case $B=5$ T, the other lines show the decomposition into lattice specific heat (line with positive curvature), field-induced linear term (straight line), and Schottky three-level anomaly (line with negative curvature). Inset: relative deviations from the fit.

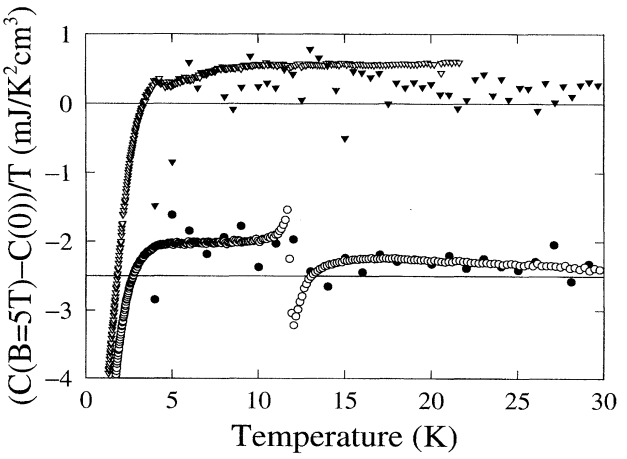

FIG. 10. Variation of the specific heat between 0 and 5 T according to direct calorimetric measurements (open symbols), and according to magnetization measurement, Eq. (5) (closed symbols). Upper set of data: sample 916c. Lower set of data, shifted by −2.5 mJ/(K^2 cm^3) for clarity: sample 918c, which orders at $T_N\approx 12$ K.

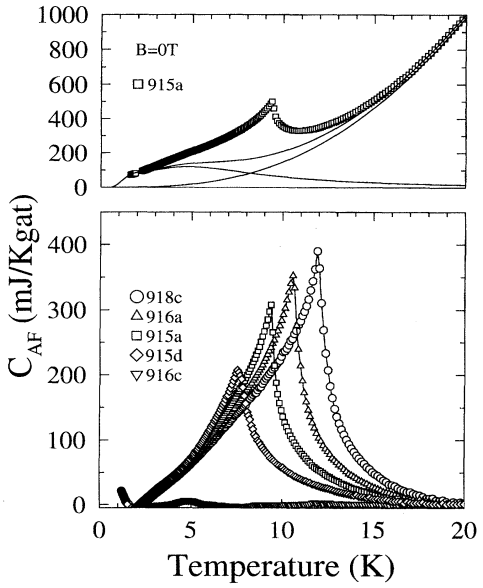

FIG. 11. Upper panel: Specific heat versus temperature for sample 915a in zero field. The solid lines are the lattice, Schottky, and the sum of both contributions. Lower panel: AF part of the zero-field specific heat vs temperature for the different samples.

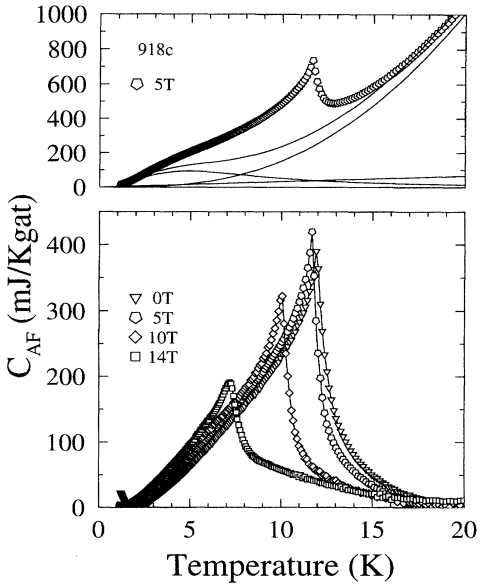

FIG. 12. Upper panel: Specific heat versus temperature for sample 918c in a magnetic field of 5 T. The solid lines are the lattice, Schottky, quasilinear term, and the sum of the three contributions. Lower panel: AF part of the field-dependent specific heat versus temperature for sample 918c.

The decomposition of the specific heat of sample 918c in a 5 T field, presented in the upper panel of Fig. 12, shows that our many-level model also describes properly the field dependence of the Schottky contribution. We emphasize that this decomposition, as well as similar decompositions for the 10 and 14 T fields, is not a fit but a simple recalculation in accordance with Eq. (2) with the parameters from Table III. The lattice contribution and the prefactor of the Schottky contribution are taken from the zero-field specific heat of the same sample, and the energy levels e_i and degeneracy factors g_i are taken from the transition-free sample 916c at corresponding fields. The values of the coefficients $\gamma(B)$ are those of sample 916c scaled by the same field-independent ratio as the Schottky prefactors. This gives strong support to the idea that the magnetic-field-induced linear term is of magnetic origin and results from the splitting of a many-level system in a field.

D. Critical behavior of the AF transition

Transition to AF order can be described in terms of critical behavior close enough to the Néel point.[26] The divergence of the specific heat is generally characterized by a small exponent (e.g., in the Ising, XY, and Heisenberg models) so that the logarithmic approximation is relevant:

$$C^{+}_{\text{trans}} = C_0 - A^{+}\ln\left(\frac{T}{T_N}-1\right), \quad T>T_N, \tag{6a}$$

$$C^{-}_{\text{trans}} = C_0 + \Delta C - A^{-}\ln\left(1-\frac{T}{T_N}\right), \quad T<T_N, \tag{6b}$$

where the $+$ and $-$ indices refer to $T>T_N$ and $T<T_N$, respectively. The amplitude ratio A^{+}/A^{-} gives information on the universality class of the transition. We plot in Fig. 13 the magnetic part C_{AF} of the specific heat vs $\ln|1-T/T_N|$. For clarity, only samples 918c and 915a are shown. In a small interval close to T_N, the data collapse on straight lines, as required by Eq. (6). For sample 918c, the validity range is $|T-T_N|/T_N<0.1$, excluding a window of ± 0.2 K near T_N. In this interval, the amplitude ratio is $A^{+}/A^{-} = 1.60\pm 0.05$ (see Table III for the other samples). The scaling theory predicts an amplitude ratio $A^{+}/A^{-}=1$ for the two-dimensional (2D) Ising model, 1.52 to 1.58 for the isotropic 3D Heisenberg model, 1.03 to 1.08 for the planar 3D XY model, and 0.52 to 0.54 for the uniaxial 3D Ising model.[26] The present data indicate that the AF transition rather belongs to the 3D Heisenberg universality class.

E. Oxygen dependence of T_N

Neutron-scattering measurements show that the AF transition comes from the long-range ordering of the Cu_6O_{12} rings,[6] with a moment of $0.89(5)\mu_B$ per Cu in the Cu_6O_{12} rings. These rings are completely occupied clusters according to Paulus *et al.*,[7] independently of the oxygen stoichiometry. Hence the variation of T_N is more probably connected with indirect effects through a charge redistribution process. The latter in turn leads to a variation of chemical bond lengths and/or angles, which are especially important for ferromagnetic superexchange interactions inside the magnetically active clusters.[6] Although the maximum variation of the lattice constant vs oxygen content does not exceed 0.15%, we cannot exclude changes of intercluster distances that can also affect the antiferromagnetic interaction between neighboring clusters. An alternative simpler interpretation will, however, be proposed below.

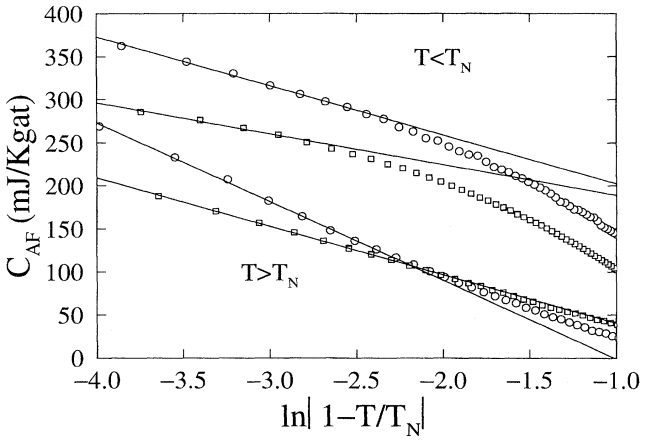

FIG. 13. Plot of the AF contribution to the specific heat in the critical region versus the logarithm of the reduced temperature. Circles: sample 918c. Squares: sample 915a. The full lines show fits of the critical behavior, Eq. (6).

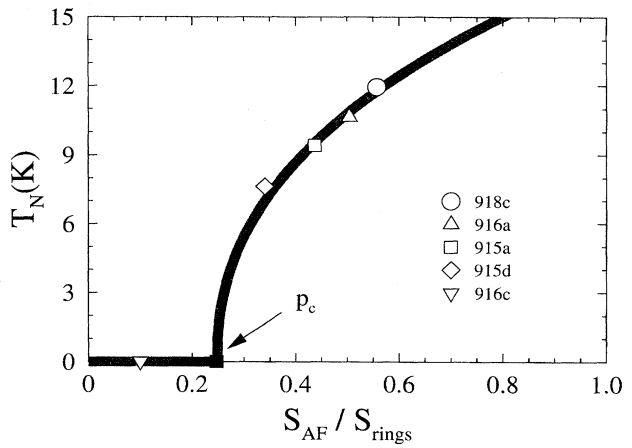

FIG. 14. Néel temperature versus the fraction of Cu_6O_{12} rings that order antiferromagnetically, S_{AF}/S_{rings}. The percolation limit $p_c = 24.7\%$ for a 3D system (Ref. 28) is indicated by an arrow. The full line is a guide for the eye.

F. Relation between effective model and structural entities

Having decomposed the measured specific heat into three contributions, i.e., lattice, Schottky, and AF transition, for all oxygen concentrations, we can now discuss the structural aspect of the proposed effective model of many-level magnetic systems and its relation to the AF ordering. Figure 11 shows the gradual decrease of the amplitude of the AF transition with increasing oxygen concentration, whereas the number of many-level systems responsible for the Schottky term follows an opposite behavior (Table III). The maximal expected entropy associated with all Cu_6O_{12} rings can be estimated as $S_{rings} = 360$ mJ/(K g-at.). The entropy S_{AF} associated with the AF transitions was calculated by integration of the curves given in Fig. 11 (Table III) from 2 K upwards. The entropy saturates below 20 K for all samples, and decreases with increasing oxygen doping. The fact that about 80% of the entropy is obtained below T_N indicates long-range ordering. Although the full magnetic entropy S_{AF} given by integration should, generally speaking, be considered with some caution owing to the uncertainty in the lattice baseline, it appears reasonably trustworthy in the present case because it scales tightly with the well-determined entropy S_{T_N} integrated up to T_N, and also because the ratio $(S_{AF} - S_{T_N})/S_{T_N} \approx 0.2$ compares well with the ratio 0.17 found in another 3D Heisenberg antiferromagnet with a large spin, namely, MnF_2.[27] We consider therefore that the variation in the full AF entropy, or more precisely the ratio S_{AF}/S_{rings}, reflects the fraction of Cu_6O_{12} rings involved in the AF long-range order. It is concluded that only about one-half of the rings contribute in sample 918c. This ratio decreases with oxygen loading down to about 35% for sample 915d, the last one in our series having an AF transition.

The remaining part of the rings in the structure, i.e., $1 - S_{AF}/S_{rings}$ (Table III), is free of AF order and can contribute to the many-level system together with the $Cu_{18}O_{24}$ spheres. The latter structural clusters supposedly have the largest spin,[6] but it would be impossible to explain the Schottky contribution based on these blocks alone, since their maximal magnetic entropy, $S_{sphere} = 136$ mJ/(K g-at.), turns out to be much smaller than the measured entropy S_{Sch} in the Schottky anomaly for all five samples. These values of S_{Sch}, given in Table III, were obtained by integrating C_{Sch}/T vs T from 0 to 30 K. If we assume that, because of their large spin, all $Cu_{18}O_{24}$ spheres participate in the many-level system at any oxygen content, the ratio $(S_{Sch} - S_{sphere})/S_{ring}$ gives the fraction of the Cu_6O_{12} rings that contributes to the Schottky anomaly (Table III). It is interesting to note that the prefactor NN_Ak_B of the total Schottky contribution, or equivalently the Schottky entropy or the number of many-level systems, grows proportionally to the number of Cu_6O_{12} rings which do not participate in the AF long-range ordering; but only approximately half of these free rings appear to be involved directly in the many-level magnetic subsystem. It seems reasonable to think that the extra oxygen atoms incorporated into the $BaCuO_x$ structure introduce a disorder responsible for the frustration of AF order. A plot of the Néel temperature vs S_{AF}/S_{rings}, i.e., the concentration of the AF ordered rings, gives a phase diagram typical of a diluted magnetic system (Fig. 14). We can speculate then that AF long-range order disappears when the concentration of the structural blocks unperturbed by extra oxygen falls below the percolation limit, $p_c = 24.7\%$ for the three-dimensional case.[28] Sample 915d with $S_{AF}/S_{rings} \approx 35\%$ seems to be rather close to this critical concentration.

The last remarkable feature of the magnetic properties of $BaCuO_x$ is a field-induced quasilinear term in the specific heat resulting from the appearance of a spin pseudoband. This effect increases with the oxygen content, and is somewhat reminiscent of the formation of a conducting band in high-T_c copper oxides as a result of hole doping. As a matter of fact, the same triggering mechanism, namely, a charge transfer process, could be responsible for both phenomena.

VI. CONCLUSIONS

The stability of the $BaCuO_x$ phase mapped over a wide range of temperature and oxygen pressure (10^{-5}–10^3 bar) is found to agree with the theoretical prediction of Voronin and Degterov.[19] In accordance with this phase diagram, single-

phase $BaCuO_x$ samples with different oxygen contents suitable for the magnetic and specific heat measurements in magnetic fields up to 14 T were prepared and characterized with x-ray diffraction and EDAX techniques as well as with optical microscopy.

Following previous magnetic and neutron-diffraction experiments,[6] we have derived a simple model of many-level magnetic systems which effectively reproduces the behavior of the low-temperature specific heat and its variation as a function of oxygen content and magnetic field. We showed how these many-level magnetic systems can be related to the Cu_6O_{12} and $Cu_{18}O_{24}$ structural blocks of $BaCuO_x$.

We analyzed the effect of both oxygen concentration and magnetic field on the AF long-range order, and found that the transition in zero fields belongs to the 3D isotropic Heisenberg universality class. The magnetic field reduces the Néel temperature in a quadratic way, as usual for antiferromagnets;[29] the possible occurrence of a spin-flop transition was not investigated. We finally argue that long-range AF order disappears with increasing oxygen concentration when the number of structural blocks involved in the long-range AF order decreases below the 3D percolation limit.

ACKNOWLEDGMENTS

The authors are grateful to F. Liniger and A. Naula for their technical assistance. Special thanks are due to Dr. A. Erb for fruitful discussions on the phase diagram, to Dr. G. Müller-Vogt for chemical analyses, and to Dr. F. Bonhomme for his expert help in crystallographic characterization. This work was supported by the Fonds National Suisse de la Recherche Scientifique.

*Author to whom correspondence should be addressed.
†Permanent address: Institute for Metal Physics, Russian Academy of Sciences, 620219 Ekaterinburg, Russia.

[1] D. Eckert, A. Junod, A. Bezinge, T. Graf, and J. Muller, J. Low Temp. Phys. **73**, 241 (1988); D. Eckert, A. Junod, T. Graf, and J. Muller, Physica C **153-155**, 1038 (1988).
[2] E. Janod, A. Junod, K.-Q. Wang, G. Triscone, R. Calemczuk, and J.-Y. Henry, Physica C **234**, 269 (1994).
[3] B. F. Woodfield, R. A. Fisher, N. E. Phillips, R. Caspary, P. Hellmann, F. Steglich, and T. Wolf, Physica C **234**, 380 (1994).
[4] R. Kipka and H. K. Müller-Buschbaum, Z. Naturforsch. Teil **32**, 121 (1977).
[5] W. Gutau and H. K. Müller-Buschbaum, J. Less-Common Met. **152**, L11 (1989).
[6] Z.-R. Wang, X.-L. Wang, J. A. Fernandez-Baca, D. C. Johnston, and D. Vaknin, Science **264**, 402 (1994).
[7] E. F. Paulus, G. Wltschek, and H. Fuess, Z. Kristallogr. **209**, 586 (1994); E. F. Paulus, G. Miehe, H. Fuess, I. Yehia, and U. Löchner, J. Solid State Chem. **90**, 17 (1991).
[8] R. Ahrens, T. Wolf, H. Wohl, H. Rietschel, H. Schmidt, and F. Steglich, Physica C **153-155**, 1008 (1988).
[9] S. Erikson, L.-G. Johansson, L. Boerjesson, and M. Kakihana, Physica C **162-164**, 59 (1989).
[10] R. Kuentzler, Y. Dossmann, S. Villminot, and S. El Hadigui, Solid State Commun. **65**, 1529 (1988).
[11] T. Sasaki, O. Nakatsu, N. Kobayashi, A. Tokiwa, M. Kikuchi, A. Liu, K. Hiraga, Y. Syono, and Y. Muto, Physica C **156**, 395 (1988).
[12] D. Sanchez, A. Junod, J.-Y. Genoud, T. Graf, and J. Muller, Physica C **200**, 1 (1992).
[13] K. A. Moler, D. J. Baar, J. S. Urbach, Ruixing Liang, W. N. Hardy, and A. Kapitulnik, Phys. Rev. Lett. **73**, 2744 (1994).
[14] T. Graf, G. Triscone, A. Junod, and J. Muller, J. Less-Common Met. **170**, 359 (1991); T. Graf, A. Junod, D. Sanchez, G. Triscone, and J. Muller, Physica C **185-189**, 473 (1991).
[15] A. Sakthivel and R. A. Young, Computer program DBWS-9006, School of Physics, Georgia Institute of Technology, Atlanta, GA 30332, 1990.
[16] J.-Y. Genoud, T. Graf, G. Triscone, and A. Naula, Rev. Sci. Instrum. **65**, 3829 (1994).
[17] W. Wong-Ng and L. P. Cook, Powder Diffraction **9**, 280 (1994).
[18] A. Erb, T. Biernath, and G. Müller-Vogt, J. Crystal Growth **132**, 389 (1993).
[19] G. F. Voronin and S. A. Degterov, J. Solid State Chem. **110**, 50 (1994).
[20] T. B. Lindemer, F. A. Washburn, and C. S. MacDougall, Physica C **196**, 390 (1992).
[21] M. T. Weller and D. R. Lines, J. Chem. Soc. Chem. Commun. **8**, 484 (1989).
[22] E. I. Leyarovski, L. N. Leyarovska, Chr. Popov, and O. Popov, Cryogenics **28**, 321 (1989).
[23] B. Revaz *et al.* (unpublished).
[24] A. P. Ramirez, R. J. Cava, G. P. Espinosa, J. P. Remeika, B. Batlogg, S. Zahurak, and E. A. Rietman, in *High-Temperature Superconductors*, edited by M. B. Brodsky, R. C. Dynes, K. Kitazawa, and H. L. Tuller, MRS Symposia Proceedings No. 99 (Materials Research Society, Pittsburgh, 1988), p. 459.
[25] According to the third law of thermodynamics, the ground state should be nondegenerate, but in any statistical model the splitting must be very small.
[26] V. Privman, P. C. Hohenberg, and A. Aharony, in *Phase Transitions and Critical Phenomena*, edited by C. Domb and J. L. Lebowitz (Academic, London, 1991), Vol. 14, p. 1.
[27] J. W. Stout and E. Catalano, J. Chem. Phys. **23**, 2013 (1955).
[28] R. B. Stinchcombe, in *Phase Transitions and Critical Phenomena*, edited by C. Domb and J. L. Lebowitz (Academic, London, 1983), Vol. 7, p. 151.
[29] L. J. de Jongh and A. R. Miedema, Adv. Phys. **23**, 1 (1974).

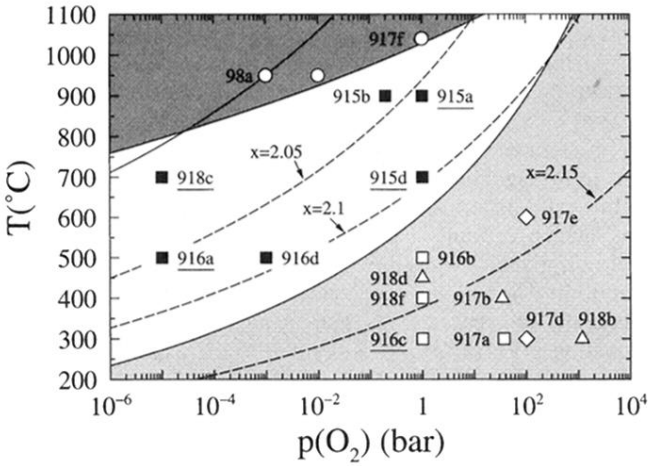

FIG. 2. Location of the various $BaCuO_x$ samples in the $p(O_2)$-T equilibrium diagram. The predicted stability domain of $BaCuO_x$ (Ref. 19) is bordered by the lower gray region and by the full line through sample 98a. The upper gray region is bordered by the solidus line (Ref. 20). The locus of equal oxygen concentration is shown by dashed lines for $x = 2.05$, 2.1, and 2.15 (Ref. 20). Each symbol indicates the oxygen pressure and the annealing temperature prior to quenching. Squares: single phase $BaCuO_x$. Triangles: partially decomposed samples. Diamonds: completely decomposed samples showing no residual $BaCuO_x$. Circles: melted samples. Full symbols: samples within the predicted stability limits. Outside of this region (open symbols), the crystal structure is expected to depend on the annealing time.

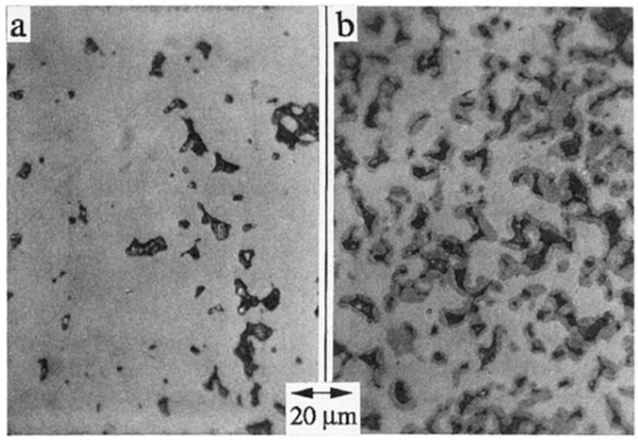

FIG. 3. (a) Optical micrograph of the pure sample 915a; the dark regions are pores. (b) Partially decomposed sample 918d; the pores are surrounded by a dark phase identified as $Ba_2Cu_3O_x$.